

Enhanced picosecond terahertz wave generation based on cascade effects in a terahertz parametric generator

Jingxi Zhang(张敬喜), Yuye Wang(王与烨), Bingfeng Xu(徐炳烽), Kai Chen(陈锴), Zikun Liu(刘紫鲲), Hongru Ma(马鸿儒), Degang Xu(徐德刚), and Jianquan Yao(姚建铨)
Citation: Chin. Phys. B, 2024, 33 (**8**): 084203. DOI: 10.1088/1674-1056/ad47b0

What follows is a list of articles you may be interested in

Gigahertz frequency hopping in an optical phase-locked loop for Raman lasers

Dekai Mao(毛德凯), Hongmian Shui(税鸿冕), Guoling Yin(殷国玲), Peng Peng(彭鹏), Chunwei Wang(王春唯), and Xiaoji Zhou(周小计)
Chin. Phys. B, 2024, 33 (**2**): 024209. DOI: 10.1088/1674-1056/ad174b

Finesse measurement for high-power optical enhancement cavity

Xin-Yi Lu(陆心怡), Xing Liu(柳兴), Qi-Li Tian(田其立), Huan Wang(王焕), Jia-Jun Wang(汪嘉俊), and Li-Xin Yan(颜立新)
Chin. Phys. B, 2024, 33 (**1**): 014205. DOI: 10.1088/1674-1056/acd8ad

Milli-Joule pulses post-compressed from 14 ps to 475 fs in bulk-material multi-pass cell based on cylindrical vector beam

Xu Zhang(张旭), Zhaohua Wang(王兆华), Xianzhi Wang(王羡之), Jiawen Li(李佳文), Jiajun Li(李佳俊), Guodong Zhao(赵国栋), and Zhiyi Wei(魏志义)
Chin. Phys. B, 2023, 32 (**10**): 104206. DOI: 10.1088/1674-1056/acd5c6

Continuous-wave optical enhancement cavity with 30-kW average power

Xing Liu(柳兴), Xin-Yi Lu(陆心怡), Huan Wang(王焕), Li-Xin Yan(颜立新), Ren-Kai Li(李任恺), Wen-Hui Huang(黄文会), Chuan-Xiang Tang(唐传祥), Ronic Chiche, and Fabian Zomer
Chin. Phys. B, 2023, 32 (**3**): 034206. DOI: 10.1088/1674-1056/ac873e

Estimation of far-field wavefront error of tilt-to-length distortion coupling in space-based gravitational wave detection

Ya-Zheng Tao(陶雅正), Hong-Bo Jin(金洪波), and Yue-Liang Wu(吴岳良)
Chin. Phys. B, 2023, 32 (**2**): 024212. DOI: 10.1088/1674-1056/aca9c5

Enhanced picosecond terahertz wave generation based on cascade effects in a terahertz parametric generator

Jingxi Zhang(张敬喜)[1,2], Yuye Wang(王与烨)[1,2,†], Bingfeng Xu(徐炳烽)[1,2], Kai Chen(陈锴)[1,2], Zikun Liu(刘紫鲲)[1,2], Hongru Ma(马鸿儒)[1,2], Degang Xu(徐德刚)[1,2], and Jianquan Yao(姚建铨)[1,2]

[1] *School of Precision Instruments and Optoelectronics Engineering, Tianjin University, Tianjin* 300072, *China*
[2] *Key Laboratory of Optoelectronic Information Technology (Ministry of Education), Tianjin University, Tianjin* 300072, *China*

(Received 15 March 2024; revised manuscript received 22 April 2024; accepted manuscript online 6 May 2024)

Enhanced terahertz wave generation via a Stokes cascade process has been demonstrated using picosecond pulse pumped terahertz parametric generation at 1 kHz repetition rate. Clear cascade saturation of terahertz output was observed, and the corresponding cascade-Stokes spectra were analyzed. The maximum terahertz wave average power was 22 μW under a pump power of 30 W, whereas the maximum power conversion efficiency was 8×10^{-7} under a pump power of 21 W. The THz power fluctuation was measured to be about 1% in 20 min. This THz parametric source with a relatively stable output is suitable for a variety of practical applications.

Keywords: terahertz parametric generation, stimulated polariton, cascade effect, CLN crystal

PACS: 42.60.–v, 42.65.–k, 42.65.Dr, 87.50.U– **DOI:** 10.1088/1674-1056/ad47b0

1. Introduction

The terahertz (THz) wave spectral region, lying between the microwave and the far infrared wave regions, is currently attracting widespread interest in relation to many potential applications, such as security inspection, communication, nondestructive evaluation, biomedical imaging and molecular analysis.[1,2] In the past, there has been remarkable growth in the field of terahertz sources in terms of their output power, frequency tuning range and pulse energy. However, when considering high-speed THz spectroscopy and imaging for real-world applications, high-power THz sources with high-repetition-rate operation are crucial concerns for researchers.

Among many optical methods for THz wave generation, THz wave parametric generation (TPG) and THz wave parametric oscillation (TPO) based on stimulated polariton scattering (SPS) in nonlinear crystals have attracted extensive interest due to their advantages of widely tunable monochromatic THz generation, high power and low cost at room temperature.[3] In 1969, efficient and widely tunable THz generation based on the A1-symmetry softest mode in $LiNbO_3$ (LN) was first studied.[4] To date, many schemes of TPG have been reported to improve the THz output power, e.g., using quasi-phase-matching schemes in LN crystals,[5] surface-emitting configurations,[6] pulsed or continuous wave injection-seeding configurations,[7,8] and intracavity geometry.[9,10] Considering that the damage threshold of LN crystal is relatively low and the pump power threshold is high due to the strong absorption by the LN crystal in the THz region, most of the research has focused on low-repetition-rate nanosecond (ns) 1064 nm pumping. A high-repetition-rate THz source based on ns 1064 nm pumping LN crystal has been reported with a peak power of only about 1 W level.[11] And the LN crystal is still easily damaged under the strong ns 1064 nm excitation. In particular, the performance of ns pumped TPG still has some limitations due to the undesirable stimulated Brillouin scattering (SBS) effect. As a picosecond (ps) pulse pumped terahertz source could suppress the SBS effect and increase the conversion efficiency by about three orders of magnitude,[12] ps pulse pumped terahertz sources have been developed recently.[13–16] To obtain high-repetition-rate THz operation, Aravindan *et al.*[14] and Takida *et al.*[15] used a bow-tie cavity to generate THz waves at 80 MHz repetition rate, where the maximum THz average power was 5.4 μW and dozens of nano-Watts, respectively. In 2019, our group used a non-synchronous picosecond pulse pump configuration to generate high-repetition-rate THz waves at 1 kHz, where the oscillation of the strong first-order Stokes wave in the TPO structure could benefit the higher-order Stokes wave emission and THz wave generation. However, the cascade effect was not obvious under the single-pass TPG configuration, where the maximum THz average power was 10.8 μW.[16]

In this paper, enhanced THz wave generation has been demonstrated based on picosecond pulse pumped TPG at 1 kHz repetition rate. Clear cascade saturation of terahertz output was observed, and the corresponding cascade-Stokes spectra were analyzed, where dramatic threshold behavior per cascade-order Stokes beam appeared. The experimental results showed that the maximum THz output power was enhanced to 22 μW under 1064 nm pump power of 30 W, whereas the power conversion efficiency was 8.0×10^{-7} under

†Corresponding author. E-mail: yuyewang@tju.edu.cn

© 2024 Chinese Physical Society and IOP Publishing Ltd

pump power of 21 W. The THz power fluctuation was measured to be 1% in 20 min.

2. Experimental setup

Figure 1 shows the experimental setup for the THz wave parametric source. The pump source was a Nd:YAG picosecond laser (Daheng Atlas (Beijing) Laser Technology Co. Ltd: Sagittarius-X40) with a repetition rate of 1 kHz and a pulse width of a hundred picosecond. The telescope lenses T1 and T2 were used to reduce the diameter of the 1064 nm laser to 3 mm to improve the power density. The combination of a half wave plate (HWP) and a Brewster polarizer (BP) was used to adjust the polarization and energy of the 1064 nm laser beam. The nonlinear optical crystal was a 5 mol.% MgO-doped congruent $LiNbO_3$ crystal (MgO:CLN) with an isosceles trapezoid shape in the x–y plane. The longer base of the isosceles trapezoid was 55 mm, while the shorter base was 34.7 mm. The thickness of the MgO:CLN crystal was 10 mm. The bottom angle of the isosceles trapezoid was 65°, which guaranteed that the pump wave and Stokes wave were totally reflected at the surface of the MgO:CLN crystal. More importantly, this kind of configuration also allowed the THz wave to be perpendicular to the MgO:CLN crystal surface, which had lower loss compared to the traditional Si-prism coupling configuration. As the time constant of the Golay cell detector (TYDEX, Inc.:GC-1P) is larger than 10 ms and the optimum operation frequency is less than 50 Hz, the emitted THz wave was chopped with an optical chopper (Stanford Research Systems: SR540) at a frequency of 10 Hz (50% duty cycle). The optical responsivity of the Golay cell detector at a repetition rate of 10 Hz was calibrated by an optically pumped THz laser (FIRL100, Edinburgh Instruments Ltd) to be 41.28 kV/W. Moreover, to block the direct injection of the intense pump wave and Stokes wave into the Golay cell detector, a 0.7 mm thick transmittance-calibrated black polyethylene (PE) sheet was used before the Golay cell as the THz filter. In addition, the black PE sheet was adopted as the THz wave attenuator to avoid saturation of the THz detector. The wavelength of the Stokes wave was measured using an optical spectrum analyzer (OSA, Yokogawa: AQ6373). The THz frequency can be calculated from the frequency difference between the pump and Stokes wavelengths according to conservation of the total energy. The powers of the pump and Stokes waves were measured by a power meter (Ophir: Nova II).

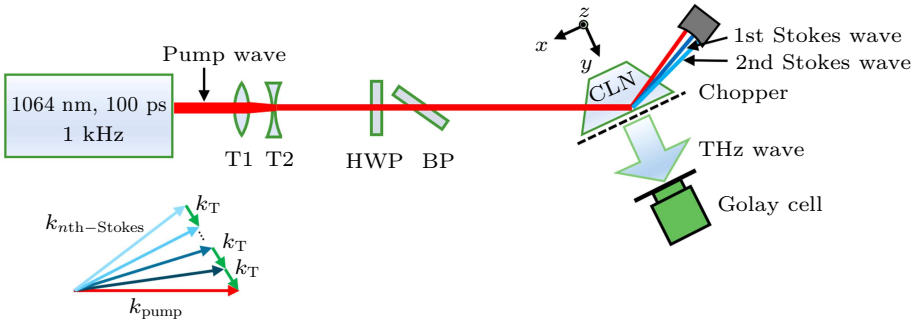


Fig. 1. The experimental setup of the picosecond pulse pumped terahertz parametric generation source.

3. Results and discussion

To realize that the SBS effect is minimized in the LN crystal and the gain of the SPS process is maximized, it is necessary to have a pulse duration of less than 1 ns.[12] Figure 2(a) shows the pulse duration of the ps pump laser, which is about 112 ps (FHWM) in the experiment. Figure 2(b) indicates the beam profile near the laser outlet. According to the measurement, the diameter of the laser in the X direction was 5.028 mm, and the diameter in the Y direction was 4.862 mm. And the beam quality M^2 factors were 1.8 (X) and 1.7 (Y).

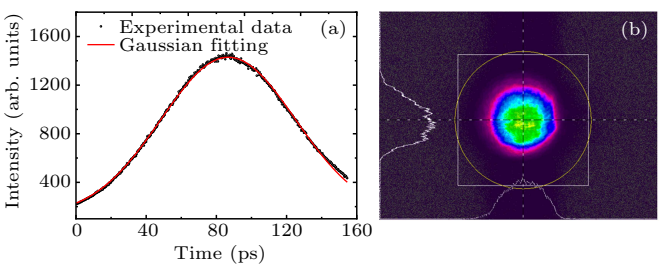


Fig. 2. The characteristics of the ps pulse. (a) The temporal waveform. (b) The beam quality and intensity profile.

Figure 3 shows the THz wave output characteristics and power conversion efficiency under different pump powers, where the power conversion efficiency is calculated based on the THz output power divided by the input 1064 nm pump power. Overall, the THz output power was increased with the 1064 nm pump power increasing from 7 W to 30 W, and the threshold pump power was 7 W. But there was a saturation phenomenon during the process. It is clearly seen from Fig. 3 that the THz wave signal intensity from the Golay cell and power conversion efficiency firstly increased with the pump power increasing. When the pump power increased from 10 W to 13 W, the average power of the THz wave appeared to have a saturation tendency, whereas the power conversion efficiency showed saturation and a slightly decreasing tendency.

Here, this phenomenon is attributed to the primary SPS process. Then, when the 1064 nm pump power was increased from 13 W to 19 W, the THz average power and conversion efficiency were enhanced. When the 1064 nm pump power was larger than 19 W, the THz average power still increased with lower slope efficiency, namely, the increase rate of THz average power became slower, whereas the THz conversion efficiency achieved saturation. It can be inferred that THz photons were continuously generated and increased under higher pump power, whereas more pump power was consumed, which resulted in the saturation or decrease in the optical conversion efficiency. Therefore, it is deduced that a different conversion phenomenon, i.e., the cascade effect, occurred under higher pump power. Moreover, the maximum THz average power was 22 μW under a pump power of 30 W, corresponding to a THz power conversion efficiency of 7.3×10^{7}. The peak power reached 220 W. Comparatively, the maximum THz power conversion efficiency was 8.0×10^{-7} under a pump power of 21 W, where the corresponding photon conversion efficiency was 1.024×10^{-4}. As the damage threshold of the MgO:$LiNbO_3$ crystal is relatively low, to limit the pump power density, any further change in THz wave output power is not undertaken.

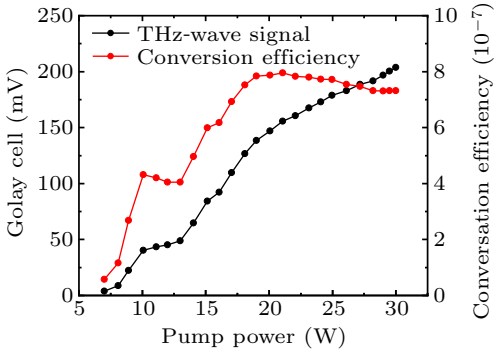


Fig. 3. THz wave output characteristics and power conversion efficiency.

Then, a receiving screen was placed behind the MgO:$LiNbO_3$ crystal to observe the spatial distribution of the pump light and Stokes light. Here, as the noncollinear phase-matching angles between the pump light and different orders of Stokes waves were different, as shown in Fig. 1, the spatial distribution of different orders of Stokes waves can be visualized by second harmonic generated green light. Figure 4(a) shows the spatial distribution of the pump and Stokes waves as the pump power was gradually increased from 7 W to 25 W. It is seen that the different-order cascading Stokes lights successively appeared as the pump power increased. When the incident pump power was 7 W, only the pump light was visible at point A. It should be mentioned that the left beam point B was the pump light reflected from the crystal inside, which can always be observed. In particular, when the pump power was 10 W, the first-order Stokes wave was visible around point C. Then, the second-order Stokes wave appeared around point D under the pump power of 15 W. The third- and fourth-order Stokes waves successively became visible around points E and F. It is clear that the spots were getting much brighter as the pump power was increased. Meanwhile, the intensity of the spots progressively intensified with the increasing pump power and the angle between high-order Stokes waves gradually became larger due to their different noncollinear phase-matching conditions.

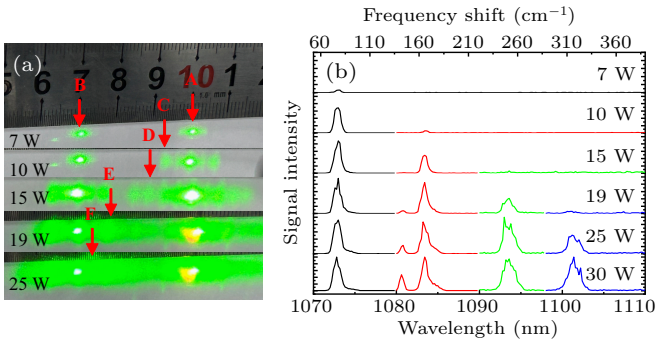


Fig. 4. (a) Spatial distribution of the pump and different orders of Stokes waves; (b) spectra of the cascaded Stoke waves under 7 W, 10 W, 15 W,19 W, 25 W, 30 W of the pump laser.

Spectral measurements were conducted on the Stokes lights in Fig. 4(a) and the exact position of the different-order Stokes lights was confirmed. Figure 4(b) shows the spectra of the pump and Stokes waves as the pump power was gradually increased from 7 W to 30 W, where the optical spectrometer was gradually moved from point A to point F due to the different positions of different orders of Stokes lights. The spectral lines of different-order Stokes waves under different pump powers were normalized using the intensity of maximum Stokes wave power to reflect the frequency shift relationship more clearly.

As shown in Fig. 4(b), at the threshold pump power of 7 W, the first-order Stokes wave with a central wavelength of 1072.8 nm was generated, which corresponds to the frequency shifts (i.e., THz wavenumbers) of 77 cm^{-1}. As the wavelength of Stokes light was 1072.4–1073.6 nm, the generated THz frequency was 1.89–2.98 THz. When the pump power was 10 W, the second-order Stokes wave (1082.8–1084 nm) with a central wavelength of 1083.4 nm appeared. It is known that the strong first-order Stokes wave can benefit the higher-order Stokes wave emission and THz wave amplification.[16,17] The frequency of the THz wave, generated by the primary SPS process and the nth-order Stokes-light-induced cascade SPS process, can be theoretically expressed as

$$\begin{aligned} f_{\mathrm{THz}} &= \frac{c}{\lambda_{\mathrm{pump}}} - \frac{c}{\lambda_{1\mathrm{st-Stokes}}} = \frac{c}{\lambda_{1\mathrm{st-Stokes}}} - \frac{c}{\lambda_{2\mathrm{nd-Stokes}}} \\ &= \cdots = \frac{c}{\lambda_{n-\mathrm{Stokes}}} - \frac{c}{\lambda_{(n+1)-\mathrm{Stokes}}}, \end{aligned} \tag{1}$$

where f_{THz} is the frequency of the THz wave, and λ_{pump}, $\lambda_{1\mathrm{st-stokes}}$, $\lambda_{2\mathrm{nd-Stokes}}$, and $\lambda_{n-\mathrm{Stokes}}$ represent the wavelengths

of the pump light, the first-order Stokes light, the second-order Stokes light, and the *n*th-order Stokes light, respectively. Compared with the saturation phenomenon of THz power and conversion efficiency in Fig. 3, it can be deduced that THz wave generation from the secondary SPS process still exhibits threshold behavior. Specifically, secondary THz generation can be realized until the intensity of the second-order Stokes wave is strong enough. Similarly, when the pump power is increased from 15 W to 19 W, it can be observed that the third-order Stokes wave of 1093.4–1093.8 nm changed from indistinctness to apparentness. As the THz output power and conversion efficiency were increased in this pump-power range, as shown in Fig. 3, the primary and secondary SPS conversions play the main roles in THz wave generation. In the cascading process, more than one THz photon is generated from the depletion of a single pump photon; therefore, they will break the limit of quantum defect according to Manley–Rowe relations and improve the photon conversion efficiency, which is in good agreement with the experimental results in Fig. 3. With the increase in pump power to 25 W, the fourth-order Stokes wave 1100.2–1102.2 nm with a central wavelength of 1101.4 nm was generated, which corresponds to the frequency shifts of 319 cm^{-1}. When the pump power continuously increased to 30 W, the higher-order Stokes wave was not observed. The reason for this is that the intensity of the fourth-order Stokes wave was relatively weak due to the low efficiency of the cascade conversion, even when the pump power was increased. Furthermore, the interaction area between the fourth-order Stokes wave and THz wave in the crystal became smaller due to the noncollinear phase-matching conditions, which induced the gain to be less than the SPS threshold. Additionally, the phase mismatching may exceed the gain bandwidth.[13] Here, it is worth mentioning that, although the fourth-order Stokes wave was observed in our experiment, because the THz conversion efficiency was saturated when the pump power was higher than 19 W in Fig. 3, it can be inferred that the third and fourth SPS processes have only a small effect on THz generation, whereas more pump power should be consumed for cascade-effect generation. This is in good agreement with the theoretical calculation in Ref. [17].

Furthermore, the spectral widths (FWHM) for each spectrum in Fig. 4(b) were calculated via Gaussian fitting, and are summarized in Table 1. From Fig. 4(b) and Table 1, we found that the linewidths of each order of Stokes wave were broadened when the pump power was increased, where Stokes wavelengths under 30 W pumping power were 1071.6–1075.8 nm, 1077.6–1082.2 nm, 1092–1095.4 nm, and 1099–1103.2 nm. This can be attributed to the fact that the phase-matching bandwidth is wider and the angular acceptance is larger as the pump intensity increases.[18] This means that the THz frequency also became wider under higher pump power.

Table 1. Linewidth of Stokes waves.

Power	1st-order Stokes (nm)	2nd-order Stokes (nm)	3rd-order Stokes (nm)	4th-order Stokes (nm)
7 W	0.68			
1 W	0.86	0.66		
15 W	0.92	0.69	0.27	
19 W	1.01	0.89	1.27	1.14
25 W	1.04	1.05	1.55	1.55
3 W	1.01	0.91	1.63	1.64

Figure 5(a) shows the signal of the Golay cell detector at a fixed chopping frequency of 10 Hz. Considering that the response time of the Golay cell detector is always larger than 10 ms, the chopping frequency of the THz signal was set to 10 Hz, where the detector has a higher detection sensitivity. The chopped THz wave signal was similar to the chopped signal of a continuous THz wave signal, which differs from the traditional pulsed signal. THz average power can be calculated as

$$P_{\text{avg}} = \frac{2V}{T \cdot R}, \tag{2}$$

where P_{avg} is the THz wave average power, V is the voltage of the Golay cell, T is the transmittance of PE and R represents the responsibility of the Golay cell at 10 Hz. Because the duty cycle of the chopper was set to 50%, the factor 2 should be multiplied together to get P_{avg}. Figure 5(b) displays the THz wave signal from the Golay cell recorded over a continuous period of 20 min under pump power of 30 W. The power fluctuation (RMSE) was measured to be about 1%. Considering that the instability of the pump source was 0.43%, it can be inferred that the fluctuation of the THz output can be reduced by improving the stability of the pump source.

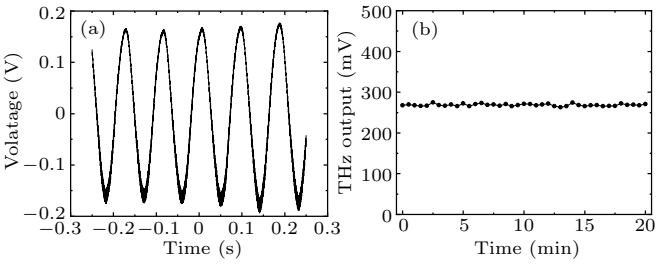


Fig. 5. (a) The THz wave signal detected by the Golay cell under a fixed chopping rate of 10 Hz; (b) the THz output fluctuation over 20 min.

4. Conclusion

In conclusion, the enhancement of terahertz wave generation via the Stokes wave cascade effect based on a TPG configuration has been demonstrated using picosecond laser pumping at 1 kHz. Cascade saturation of THz output was observed under different pump powers. The corresponding cascade-Stokes spectra were analyzed. The maximum THz output power was enhanced to 22 μW under a 1064 nm pump power of 30 W. The maximum power conversion efficiency was 8×10^{-7} under a pump power of 21 W, which could be further improved via an injection-seeding technique or THz

parametric oscillation. The THz power fluctuation was measured to be 1% in 20 min. This kind of high-repetition-rate THz source with high stability and a simple configuration is suitable for the broader THz applications.

Acknowledgements

This research was funded by the National Natural Science Foundation of China (Grant Nos. U22A20353, U22A20123, 62175182, and 62275193). The authors would like to thank Daheng Atlas (Beijing) Laser Technology Co. Ltd. for their support.

References

[1] Siegel P H 2002 *IEEE Trans. Microw. Theory Techn.* **50** 910
[2] Tonouchi M 2007 *Nat. Photon.* **1** 97
[3] Kawase K, Shikata J and Ito H 2002 *J. Phys. D* **35** R1
[4] Yarborough J M, Sussman S S, Puthoff H E, Pantell R H and Johnson B C 1969 *Appl. Phys. Lett.* **15** 102
[5] Vodopyanov K L 2006 *Opt. Express* **14** 2263
[6] Ikari T, Zhang X B, Minamide H and Ito H 2006 *Opt. Express* **14** 1604
[7] Imai K, Kawase K, Shikata J, Minamide H and Ito H 2001 *Appl. Phys. Lett.* **78** 1026
[8] Tang L H, Xu D G, Wang Y Y, Yan C, He Y X, Li J N, Zhong K and Yao J Q 2019 *Opt. Express* **27** 22808
[9] Edwards T J, Walsh D, Spurr M B, Rae C F, Dunn M H and Browne P G 2006 *Opt. Express* **14** 1582
[10] Gao F L, Zhang X Y, Cong Z H, Liu Z J, Chen X H, Qin Z G, Wang P, Xu J J, Wang W T and Zhang S J 2020 *IEEE Photonics Journal* **12** 1400109
[11] Ortega T A, Pask H M, Spence D J and Lee A J 2017 *Opt. Express* **25** 3991
[12] Nawata K, Hayashi S, Ishizuki H, Murate K, Imayama K, Takida Y, Yahia V, Taira T, Kawase K and Minamide H 2017 *IEEE Trans. Terahertz Sci. Technol.* **7** 617
[13] Hayashi S, Nawata K, Taira T, Shikata J, Kawase K and Minamide H 2014 *Sci. Rep.* **4** 5045
[14] Warrier A M, Li R, Lin J P, Lee A J, Pask H M and Spence D J 2016 *Opt. Lett.* **41** 4409
[15] Takida Y, Ohira T, Tadokoro Y, Kumagai H and Nashima S 2013 *IEEE Journal of Selected Topics in Quantum Electronics* **19** 8500307
[16] Yan C, Xu D G, Wang Y Y, Wang Z H, Wei Z Y, Tang L H, He Y X, Li J N, Zhong K, Shi W and Yao J Q 2019 *IEEE Photonics Journal* **11** 5900908
[17] Li W F, Qi F, Liu P, X Wang Y L and Li Z Y 2022 *Opt. Lett.* **47** 178
[18] Powers P E and Haus J W 2017 *Fundamentals of Nonlinear Optics* (2nd edn.) (Boca Raton: CRC Press, Taylor & Francis) pp. 139–141